Astronomy & Astrophysics manuscript no. 43685
June 8, 2022

Gaia Data Release 3: Hot-star radial velocities

R. Blomme[1]⋆, Y. Frémat[1], P. Sartoretti[2], A. Guerrier[3], P. Panuzzo[2], D. Katz[2], G. M. Seabroke[4], F. Thévenin[5], M. Cropper[4], K. Benson[4], Y. Damerdji[6,7], R. Haigron[2], O. Marchal[8], M. Smith[4], S. Baker[4], L. Chemin[9], M. David[10], C. Dolding[4], E. Gosset[7,11], K. Janßen[12], G. Jasniewicz[13], A. Lobel[1], G. Plum[2], N. Samaras[1,14], O. Snaith[2], C. Soubiran[15], O. Vanel[2], T. Zwitter[16], N. Brouillet[15], E. Caffau[2], F. Crifo[2], C. Fabre[17,3], F. Frakgoudi[2], H.E. Huckle[4], A. Jean-Antoine Piccolo[3], Y. Lasne[3], N. Leclerc[2], A. Mastrobuono-Battisti[2,18], F. Royer[2], Y. Viala[2], and J. Zorec[19]

(Affiliations can be found after the references)

Received <date>; accepted <date>

ABSTRACT

Context. The second *Gaia* data release, DR2, contained radial velocities of stars with effective temperatures up to $T_{\rm eff}$ = 6900 K. The third data release, *Gaia* DR3, extends this up to $T_{\rm eff}$ = 14 500 K.

Aims. We derive the radial velocities for hot stars (i.e. in the $T_{\rm eff}$ = 6900−14 500 K range) from data obtained with the Radial Velocity Spectrometer (RVS) on board *Gaia*.

Methods. The radial velocities were determined by the standard technique of measuring the Doppler shift of a template spectrum that was compared to the observed spectrum. The RVS wavelength range is very limited. The proximity to and systematic blueward offset of the calcium infrared triplet to the hydrogen Paschen lines in hot stars can result in a systematic offset in radial velocity. For the hot stars, we developed a specific code to improve the selection of the template spectrum, thereby avoiding this systematic offset.

Results. With the improved code, and with the correction we propose to the DR3 archive radial velocities, we obtain values that agree with reference values to within 3 km s^{-1} (in median). Because of the required S/N for applying the improved code, the hot star radial velocities in DR3 are mostly limited to stars with a magnitude in the RVS wavelength band ≤ 12 mag.

Key words. Techniques: spectroscopic – Techniques: radial velocities – Methods: data analysis – Catalogs – Surveys – Stars: massive

1. Introduction

The *Gaia* satellite (Gaia Collaboration et al. 2016b) was launched in December 2013. By continuously scanning the sky, it is collecting astrometric, photometric, and spectroscopic information on a large number of stars. A number of data releases have made part of this wealth of information public (DR1 by Gaia Collaboration et al. 2016a; DR2 by Gaia Collaboration et al. 2018; EDR3 by Gaia Collaboration et al. 2021). Now the third data release (*Gaia* DR3, Gaia Collaboration et al. 2022a) is available, which not only updates the previous releases, but also adds substantially new information, such as BP/RP spectra (De Angeli et al. 2022), astrophysical parameters (Creevey et al. 2022), and variability classification (Eyer et al. 2022). This new information also includes the radial velocities for almost 34 million stars (Katz et al. 2022), and Radial Velocity Spectrometer (RVS) spectra for almost one million stars (Seabroke et al. 2022).

The *Gaia* data are processed by the Data Processing and Analysis Consortium (DPAC; see Gaia Collaboration et al. 2016a, for details). Within DPAC, the Coordination Unit 6 (CU6) is responsible for handling the RVS spectra. Its main tasks are the reduction of the RVS data for use by other Coordination Units and for publication in the data releases, as well as the determination of the radial velocity from these spectra. A secondary task is measuring the broadening of the spectral lines. This broadening is mainly due to the (projected) rotational velocity of the star, but may also include other effects, such as macroturbulence (Frémat et al. 2022). For this reason, we use the term 'broadening velocity' rather than rotational velocity. Other uses of the spectra, such as astrophysical parameter determination, are within the remit of other DPAC Coordination Units.

This paper is one of four presenting the radial velocity results in DR3. Katz et al. (2022) present the DR3 radial velocity content in general, Gosset et al. (2022) describe the processing and performance for SB1 binary stars in detail, and Damerdji et al. (2022) does the same for SB2 binaries. The present paper focusses on the radial velocity performances of hot stars. For a scientific application in which the radial velocities play an important role, we refer to Gaia Collaboration et al. (2022b).

Data release 3 is the first data release to contain radial velocities for stars with effective temperatures above 6900 K, extending the range up to 14 500 K. The previous data release DR2 did not include these, as the quality of the results could not be guaranteed. The present paper describes how these hot-star radial velocities were derived, and the caveats that have to be taken into account in their use. For stars even hotter than 14 500 K, there remain challenges that could not be solved in DR3 and will therefore be handled in the next release, DR4.

Determining radial velocities for hot stars with the *Gaia* RVS is quite challenging. The instrument is described in detail in Cropper et al. (2018). It is a medium-resolution spectrograph ($R \approx 11\,500$) covering the wavelength range 846 – 870 nm. This rather small wavelength range has been chosen to optimise radial velocity determination for cool stars. Figure 1 shows two examples of the RVS spectrum of a hot star. The hotter star (right panel) is dominated by the hydrogen Paschen lines, with no other substantial spectral lines that can be used for radial velocity determination. The somewhat cooler star (left panel) has, in addi-

⋆ e-mail: Ronny.Blomme@oma.be

Article published by EDP Sciences, to be cited as https://doi.org/10.1051/0004-6361/202243685

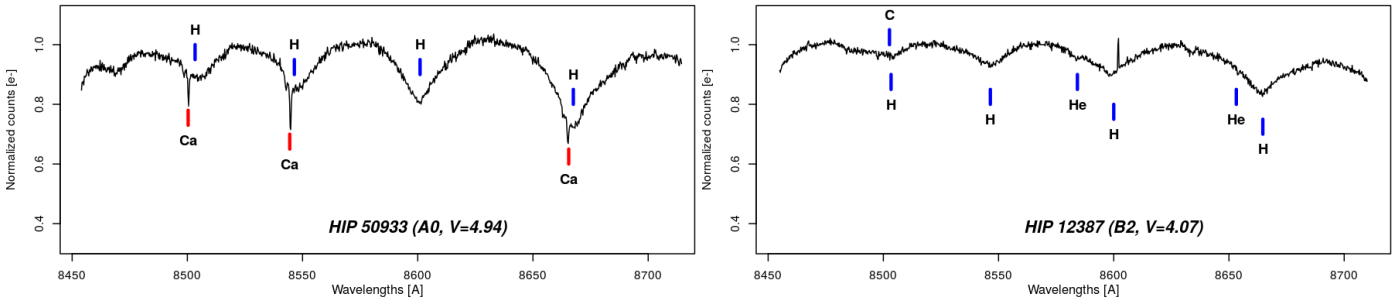

Fig. 1. Two examples of RVS spectra of hot stars (`https://www.cosmos.esa.int/web/gaia/iow_20141124`). Both stars have Paschen hydrogen lines, and the cooler star (left panel) also shows the calcium infrared triplet lines. A spectrum of the cooler star with a much higher S/N is available in the DR3 archive (Gaia DR3 1053778957742409984).

tion to the Paschen lines, also the lines from the calcium infrared triplet. While these sharper calcium lines are useful for radial velocity measurements, their proximity to the Paschen lines complicates matters.

The focal plane of *Gaia* contains four rows of three CCDs each that are dedicated to the RVS instrument. During a single transit of a star across the focal plane, three spectra are therefore taken. The integration time for a single spectrum is ∼ 4.4 s. During the 34 months of observations covered by DR3 each star has 22 of these transits on average. The information from these 22 transits can be combined to improve the signal-to-noise ratio (S/N) and thus the precision of the radial velocity determination.

In Sect. 2 we present the part of the pipeline that determines the radial velocity, and discuss the resulting hot-star radial velocities from a preliminary run of the code. Section 3 presents the specific method we implemented to improve the handling of the hot stars. In Sect. 4 we show the improvement in the resulting hot-star radial velocities. Section 5 presents the conclusions and the caveats for the user of the *Gaia* DR3 hot-star radial velocities.

2. Method

This section describes the method we used to derive the radial velocities and presents the results of a preliminary run (Sect. 2.2). As the results of this preliminary run were not satisfactory for the hot stars, an improved method was developed. This is described in Sect. 3.

2.1. STA and MTA

The processing of the RVS data consists of six pipelines (Sartoretti et al. 2022a); the four main pipelines take care of the spectrum extraction, the determination of the wavelength calibration and the background correction, and the radial velocity determination. The pipeline we are concerned with consists of two parts: single-transit analysis (STA) and multi-transit analysis (MTA). These are described in detail for DR2 in Sartoretti et al. (2018), and the description is updated for DR3 in Sartoretti et al. (2022a). Here we provide a summary of the points that are relevant for this paper. Figure 2 also provides an overview.

2.1.1. STA input

The STA part of the pipeline uses the observed spectra as input that have been wavelength-calibrated and normalised, and it uses the astrophysical parameters of the most appropriate synthetic

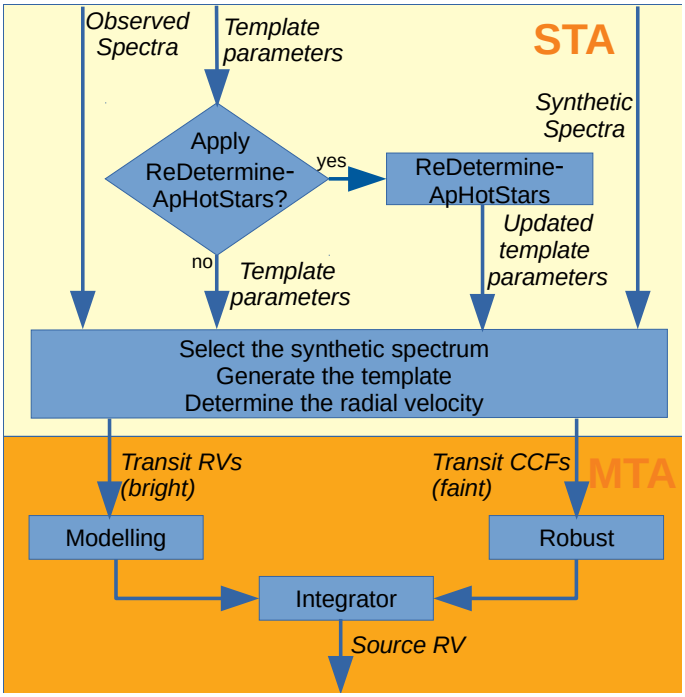

Fig. 2. Schematic overview of the STA and MTA parts of the pipeline. The input to STA consists of the normalised observed spectra and the template parameters. If ReDetermineApHotStars is applied (see Sect. 3), the template parameters are updated. The template parameters are then used to select the corresponding synthetic spectrum; this is converted into a template and used to derive the cross-correlation functions and the radial velocity for each transit. The MTA part of the pipeline takes the time series of transit radial velocities (for bright stars, i.e. `grvs_mag` ≤ 12 mag), or the time series of the transit cross-correlation functions (for faint stars, i.e. `grvs_mag` > 12 mag) to determine the stellar radial velocity.

spectrum[1]. These parameters are the effective temperature ($T_{\rm eff}$), the gravity ($\log g$), and the metallicity ([M/H]).

In principle, the astrophysical parameters are determined by Coordination Unit 8 (CU8). However, for DR3, the CU8 processing was done after the CU6 processing. The considerable

[1] We use the term 'synthetic spectrum' for the spectrum with very high resolution and very high sampling that is output from a theoretical spectrum synthesis code, and the term 'template' when such a synthetic spectrum has been convolved with the instrumental profile and possibly a line-broadening function (see Sect. 2.1.2).

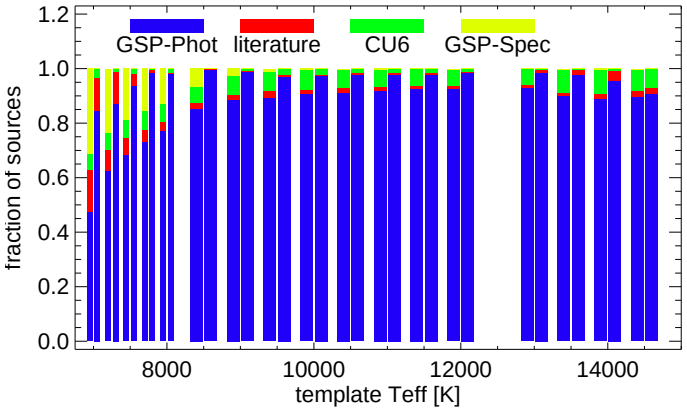

Fig. 3. Histogram showing the fraction of the stars that obtained their template parameters from the various input possibilities. The x-axis shows the template effective temperature. Each histogram bar is split into two parts: the left-hand side of each bar shows the distribution for `grvs_mag` $\leq$ 12 mag, and the right-hand side of each bar is for `grvs_mag` > 12 mag.

time needed for the processing and the validation of the results means that it is not feasible to iterate between the CU6 and CU8 processing. CU6 therefore used parameters from the preliminary CU8 run. This CU8 run used an earlier version of the GSP-Phot (Andrae et al. 2022) and GSP-Spec (Recio-Blanco et al. 2022) pipelines. GSP-Phot used DR2 photometric data instead of the better-quality and more detailed DR3 BP/RP data, while GSP-Spec used RVS spectra from the preliminary CU6 run (discussed in Sect. 2.2). These initial sets of parameters are thus intrinsically not optimal, and CU6 supplemented these data by other (non-*Gaia*) sources of parameters (Sartoretti et al. 2022a, their Table 6.4).

The input astrophysical parameters for the choice of the synthetic spectrum are determined as follows, in order of priority:

1. Parameters from the literature (Sartoretti et al. 2022a, their Table 6.4; 3.4 % of all hot stars).
2. Parameters from the preliminary run of the CU8 GSP-Spec pipeline (Recio-Blanco et al. 2022, 3.7 % of all hot stars).
3. Parameters from the preliminary run of the CU8 GSP-Phot pipeline (Andrae et al. 2022, 89.6% of all hot stars).
4. Parameters determined by CU6 from fitting the RVS spectrum with a limited set of stellar templates. (DetermineAp – Sartoretti et al. 2018, their Sect. 6.5; 3.3% of all hot stars).
5. Parameters of the Sun (with corresponding template parameters $T_{\rm eff}$ = 5500, $\log g$ = 4.5, [M/H] = 0.0; not applicable to hot stars); as we have no other information available for these stars, we use the solar parameters as a default value.

The percentages listed above are applicable for all stars that turn out to have a `rv_template_teff`[2] $\geq$ 7000 K after the improved method detailed in Sect. 3 was applied.

Based on the astrophysical parameters, the nearest synthetic spectrum is selected. The list of available synthetic spectra is given in Blomme et al. (2017). The astrophysical parameters of the synthetic spectrum (which we call template parameters from here on) are therefore usually slightly different from the true astrophysical parameters, and in the remainder of this paper, we are mainly concerned with the template parameters.

[2] We use this font style to indicate the name of columns that are available in the DR3 archive. A standard font style is used when we refer to the parameter in general, or when we refer to a parameter used in the processing (usually in STA) that was not stored in the DR3 archive.

Figure 3 shows the fraction of the hot stars (`rv_template_teff` $\geq$ 7000 K) that obtained their template parameters from each of the above possibilities. GSP-Phot is the dominant contributor. GSP-Spec, which uses the RVS spectra, does not cover the higher temperatures. This is highly relevant for this paper. The figure also shows information for hot stars with `grvs_mag` fainter than magnitude 12, but for reasons explained in Sect. 3, a cut-off magnitude 12 is applied for the DR3 archive.

2.1.2. STA processing

For a given transit, the selected synthetic spectrum is converted into a template by convolving it with the instrumental profile, and possibly with a broadening profile. For the latter, a rotational broadening kernel is used (Gray 2005), with the caveat that the line-broadening velocity can include other broadening mechanisms as well. The template is then normalised, so that it can be compared to the normalised observed spectrum.

The radial velocity and its corresponding uncertainty are then determined using three different techniques: cross-correlation by Fourier transform, Pearson correlation, and a χ^2 minimum distance (David et al. 2014). The spectra from the three CCDs that cover this single transit are processed separately (because the instrumental profile is different for the three CCDs) to derive a cross-correlation function (CCF) or a χ^2 function for each spectrum. These three functions are then combined, and the radial velocity is derived from the maximum of the combined CCF and the minimum of the combined χ^2 function. For the brighter stars, the broadening velocity is also determined; for details, we refer to Frémat et al. (2022).

The final value for the transit radial velocity is the median of the three determinations. During this processing, the spectra are also checked for the possible presence of two components and, if they are detected, the corresponding radial velocities are determined following a dedicated channel described in Damerdji et al. (2022).

2.1.3. MTA processing

In the MTA part of the pipeline, the information of all transits for a given star (with a supposed single-line spectrum) is combined. This combination is done in a different way for bright stars than for faint stars. The switch between bright and faint occurs at `grvs_mag` = 12 mag, where `grvs_mag` is the magnitude over the RVS bandpass (Sartoretti et al. 2022b).

For the bright stars (`grvs_mag` $\leq$ 12 mag), MTA corrects the STA radial velocities for the barycentric velocity and takes the median; this quantity is stored in the DR3 archive as `radial_velocity`. The corresponding uncertainty `radial_velocity_error` is derived from the uncertainty on the median (with a floor value of 0.113 km s^{-1}); for details, see Sartoretti et al. (2022a, Sect. 6.4.9).

For the faint stars (`grvs_mag` = 12 – 14 mag), MTA uses the STA cross-correlation functions determined by Fourier transform, shifts them for the barycentric velocity correction, and averages them to obtain the source cross-correlation function. From the maximum of this function, the `radial_velocity` is determined. The `radial_velocity_error` is calculated using the formula of Zucker (2003, Sect. 2.3).

In both cases, the MTA processing also provides the spectrum combined over all transits. This combined spectrum is shifted by MTA to its rest wavelength.

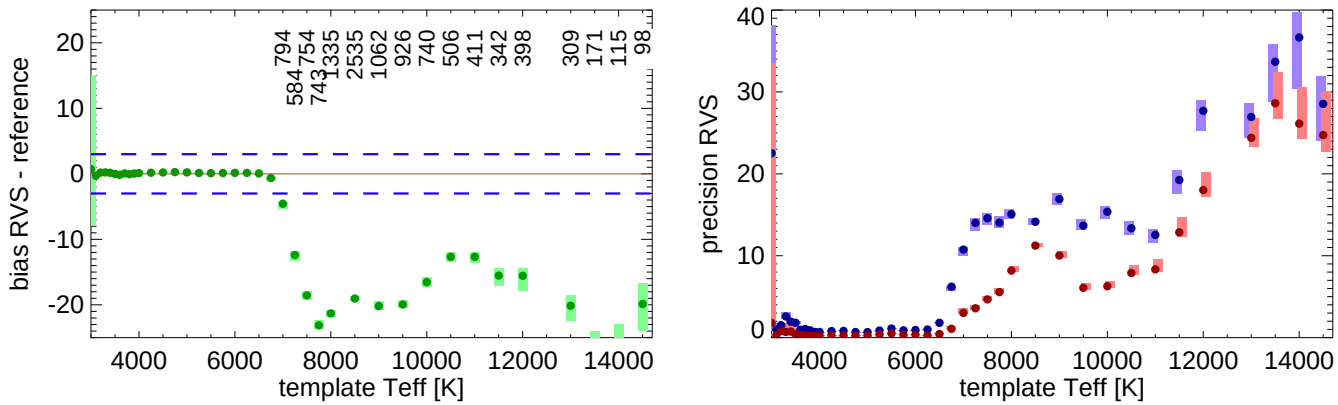

Fig. 4. Preliminary radial velocities compared to their reference values as a function of the template effective temperature. ReDetermineApHotStars was not applied to these data. The *left panel* shows the bias of the radial velocity of the stars (RVS value minus reference value). Each point on the plot presents the median of the bias of all stars having this $T_{\rm eff}$ value (the template effective temperatures take on only discrete values). The coloured bar around it gives the uncertainty on the median; in most cases, this uncertainty is smaller than the symbol. The results for cooler stars are also included in this figure to show the difference in quality of the radial velocity determination. The dashed blue lines indicate ± 3 km s^{-1}. The numbers at the top show how many stars correspond to this temperature. The *right panel* shows the precision. The blue symbols give the external uncertainty (dispersion of RVS value minus reference value), while the red symbols give the internal precision, i.e. the intrinsic uncertainty as derived by the code. The uncertainties on these values are given by the coloured bars; for the higher $T_{\rm eff}$ values, they have been offset slightly in temperature to avoid overlap. The plots include only stars with `grvs_mag` ≤ 12 mag.

2.2. Preliminary radial velocities

A preliminary run of the RVS processing pipeline revealed that the radial velocities of hot stars show a systematic offset with respect to the reference stars. The reference stars we use in this comparison are those from the literature listed in Katz et al. (2019). We also use values that were derived for cluster members using *Gaia* DR2. Although *Gaia* DR2 contains radial velocities only for cooler stars ($T_{\rm eff} \leq 6900$ K), these were used by Soubiran et al. (2018) to determine the cluster radial velocity, and the hotter stars that are members of the cluster are assigned the same velocity as the cluster.

In Fig. 4 we plot the difference between the preliminary RVS radial velocities and the reference values as a function of the template $T_{\rm eff}$. As there are a large number of stars, we condense the information by grouping the stars according to their template $T_{\rm eff}$ (which takes on only discrete values). For each template $T_{\rm eff}$, we calculate the median and the uncertainty on the median of the radial velocity difference, giving us a point and an uncertainty on the plot. The number of stars corresponding to each $T_{\rm eff}$ is listed at the top of the left panel in Fig. 4.

Figure 4 shows a clear offset of about -20 km s^{-1} for $T_{\rm eff} >$ 7000 K. The reason for this offset is a mismatch between the template and the observed spectrum. For the $T_{\rm eff}$ range we consider here, the spectra have a mixture of the calcium infrared triplet and hydrogen Paschen lines. Fig. 1 shows that three of the Paschen lines have a calcium line on their blueward side. If the template does not have the correct relative intensities of the calcium and Paschen lines, the radial velocity determination techniques will attempt to shift the theoretical Paschen lines towards the position of the observed calcium lines, leading to an incorrect, blue-shifted, velocity. A template without template mismatch would not have this problem, and the correct radial velocity would be obtained.

The right panel of Fig. 4 shows two versions of the precision. The blue symbols give the external precision: this is the half-range between the 15.85 and 84.15 percentile of the distribution of the radial velocity differences (see Katz et al. 2019, their Eqs. 4-6). The red symbols give the internal precision: this is the median value (and its uncertainty) of the radial velocity uncertainty (`radial_velocity_error`) as derived in the MTA processing (Sec. 2.1.3). The precision of stars hotter than 6500 K is considerably worse than the precision for stars at lower temperatures. The internal precision is lower than the external one, indicating that the radial velocity uncertainty is underestimated for these stars. We also checked the influence of the uncertainty of the reference values on the external precision, but this is negligible compared to the difference between external and internal precision.

3. Improved method

Because of the unsatisfactory results of the preliminary run for hot stars, we decided on a new approach, implemented as the module ReDetermineApHotStars. This module does an exhaustive brute-force search among the combination of many templates and broadening velocities to find the combination that best fits (in χ^2 sense) all transit spectra of a given star. As part of the procedure, ReDetermineApHotStars also shifts the template being explored in velocity space, and it thus also determines the transit radial velocities. However, only the updated template parameters and the broadening velocity are output from ReDetermineApHotStars; the radial velocity determination is left to the three radial velocity modules (Sect. 2.1.2).

The way the ReDetermineApHotStars module is included in the STA part of the pipeline is shown in Fig. 2. ReDetermineApHotStars is called for stars with a template $T_{\rm eff} \geq$ 7000 K. It is also called for 6500 $\leq T_{\rm eff} <$ 7000 K when the atmospheric parameters are not from literature data (see Sect. 2.1.1). We apply this procedure only to stars that are bright enough ($G_{\rm RVS} \leq 12$ mag) so that we have a sufficient S/N in the spectra.

The $G_{\rm RVS}$ value used in this procedure is not exactly the same as the `grvs_mag` available in the DR3 archive. The latter value is determined in the MTA part of the pipeline as the median of all valid transit $G_{\rm RVS}$ values (Sartoretti et al. 2022b). During the run of STA, this median value was not yet available, therefore STA used the first valid value from the list of transits.

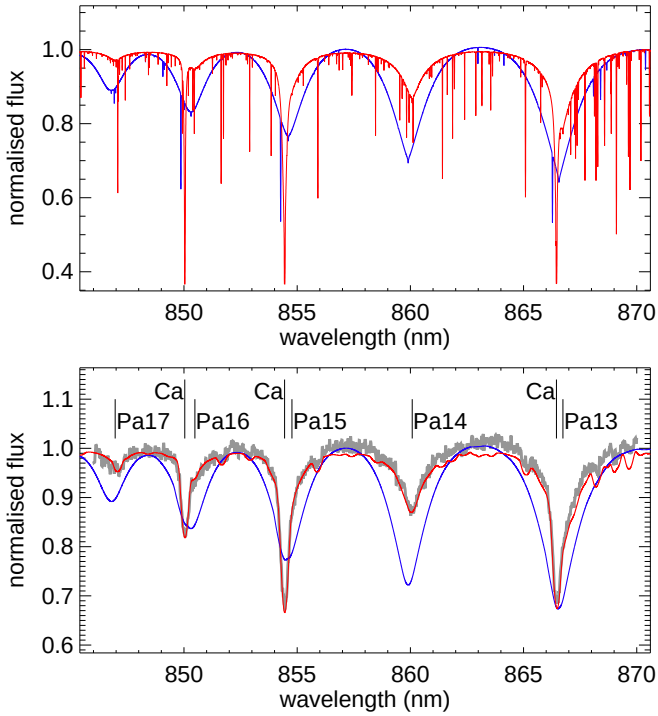

Fig. 5. Example of applying ReDetermineApHotStars. The *top panel* shows the synthetic spectra: the blue curve ($T_{\rm eff}$ = 11 500 K, $\log g$ = 4.0 dex, [M/H] = −0.50 dex) presents data to which ReDetermineApHotStars was not applied, and the red curve shows the best synthetic spectrum as determined by ReDetermineApHotStars ($T_{\rm eff}$ = 7750 K, $\log g$ = 4.5 dex, [M/H] = +0.25 dex). The *bottom panel* shows the templates derived from these synthetic spectra: they have been convolved with a broadening velocity of 100 km s^{-1} (blue curve), and 80 km s^{-1} (red curve), and with the instrumental profile. They are compared with the observed spectrum of Gaia DR3 51853419339515136 (grey curve). All spectra are at their vacuum rest wavelength, except for the blue curves, which are shifted by −60.9 km s^{-1}; this is the offset we found between the case when ReDetermineApHotStars was applied or was left unused. The template selected by ReDetermineApHotStars (red curve) clearly provides a better fit to the observed spectrum and therefore also gives a more correct radial velocity.

Table 1. Parameters of the grid of synthetic spectra used in ReDetermineApHotStars.

Code	Parameter	Range	Step
MARCS	$T_{\rm eff}$ [K]	6500 .. 8000	250
	$\log g$ [dex]	−0.5 .. +5.0	0.5
	[M/H] [dex]	−5.0 .. −3.0	1.0
		−2.5 .. −1.0	0.5
		−0.75 .. +1.0	0.25
A stars	$T_{\rm eff}$ [K]	8500 .. 12 000	500
	$T_{\rm eff}$ [K]	13 000 .. 14 500	500
	$\log g$ [dex]	+2.0 .. +5.0	0.5
	[M/H] [dex]	−0.5 .. +0.25	0.25

Because of the requirement for bright enough stars for ReDetermineApHotStars, the hot-star radial velocities in the DR3 archive are mostly limited to `grvs_mag` ≤ 12 mag. The few stars that are fainter than this are due to the difference between the value used by STA and MTA, as explained above.

Because the brute-force grid search in ReDetermineApHotStars is computing-time intensive, various optimisations are introduced in that module. We combine the observed spectra from the three CCDs into a single spectrum, so that we have to handle fewer spectra. For the combination, we use a wavelength grid with a constant step in $\log\lambda$, so that the radial velocity shifts can be made by simple index manipulation. The templates we compare with have been pre-calculated. We base them on the synthetic spectra used in the RVS processing (Blomme et al. 2017; Sartoretti et al. 2022a), selecting all those that have a $T_{\rm eff} \geq 6500$ K. The parameter ranges of the synthetic spectra we use are listed in Table 1. We convolve each synthetic spectrum with a pre-specified grid of rotational velocities and with the instrumental profile consisting of a Gaussian with the nominal RVS resolving power of 11 500. The templates are also on a wavelength grid with a constant step in $\log\lambda$.

ReDetermineApHotStars has a main loop over the set of the pre-calculated templates and an inner loop over all transits of a given star. In the inner loop, it determines the best radial velocity for each transit. It does so by exploring a range of radial velocities and calculating the χ^2 between observed spectrum and template. As part of this procedure, the normalisation of the observed spectrum is also slightly adapted to agree as well as possible with the normalisation of the template. Again, for optimisation purposes, we first use a coarse velocity grid to obtain an approximate radial velocity from the minimum χ^2. The velocity grid is then refined around this approximate result to obtain a better value, which is then even further refined by parabolic interpolation. In this way, we obtain the best radial velocity for a specific combination of pre-calculated template and transit. The inner loop then loops over all transits, and the best-fitting pre-calculated template for the star is then determined by the minimum of the χ^2 summed over all transits of that star.

As a further optimisation, we ordered the pre-calculated templates in such a way that we first explore the templates that show the highest difference among themselves (the difference between the templates is measured by the sum of the square of the flux differences). In this way, we quickly determine a template with a reasonably good χ^2 value for the star. When we proceed with the set of pre-calculated templates, we find many templates with a much higher χ^2 than the best χ^2 obtained thus far. It therefore frequently happens that as we loop over the transits, we already arrive at a summed χ^2 that is too large before we have processed all the transits of that star. We can therefore break off further processing of this specific template in the inner loop, and in this way reduce the required computing time.

An example of applying ReDetermineApHotStars is shown in Fig. 5. ReDetermineApHotStars works on the separate transit spectra, but for the example, we chose an RVS spectrum from the *Gaia* DR3 archive, which is a combination of all its transit spectra. As for all archive spectra, this spectrum was shifted to its rest wavelength, in this case, using the radial velocity based on the processing by ReDetermineApHotStars. The observed spectrum (shown in grey in the bottom panel) contains a mixture of Paschen and calcium lines. This spectrum was then compared to two templates that were derived from the synthetic spectra shown in the top panel. The template used in the preliminary run has a relatively high effective temperature ($T_{\rm eff}$ = 11 500 K) and therefore shows only weak calcium lines. When fitting such a template (blue curve) to the observed spectrum, the theoretical Paschen lines are blue-shifted in attempting to partially fit the observed calcium lines. This gives an incorrect, blue-shifted, radial velocity of −60.9 km s^{-1}. The bottom panel shows that the blue curve fits the region around Pa13 and Pa15 reasonably well, but clearly fails around Pa14, Pa16, and Pa17. ReDetermineApHotStars finds a much cooler template that has the ap-

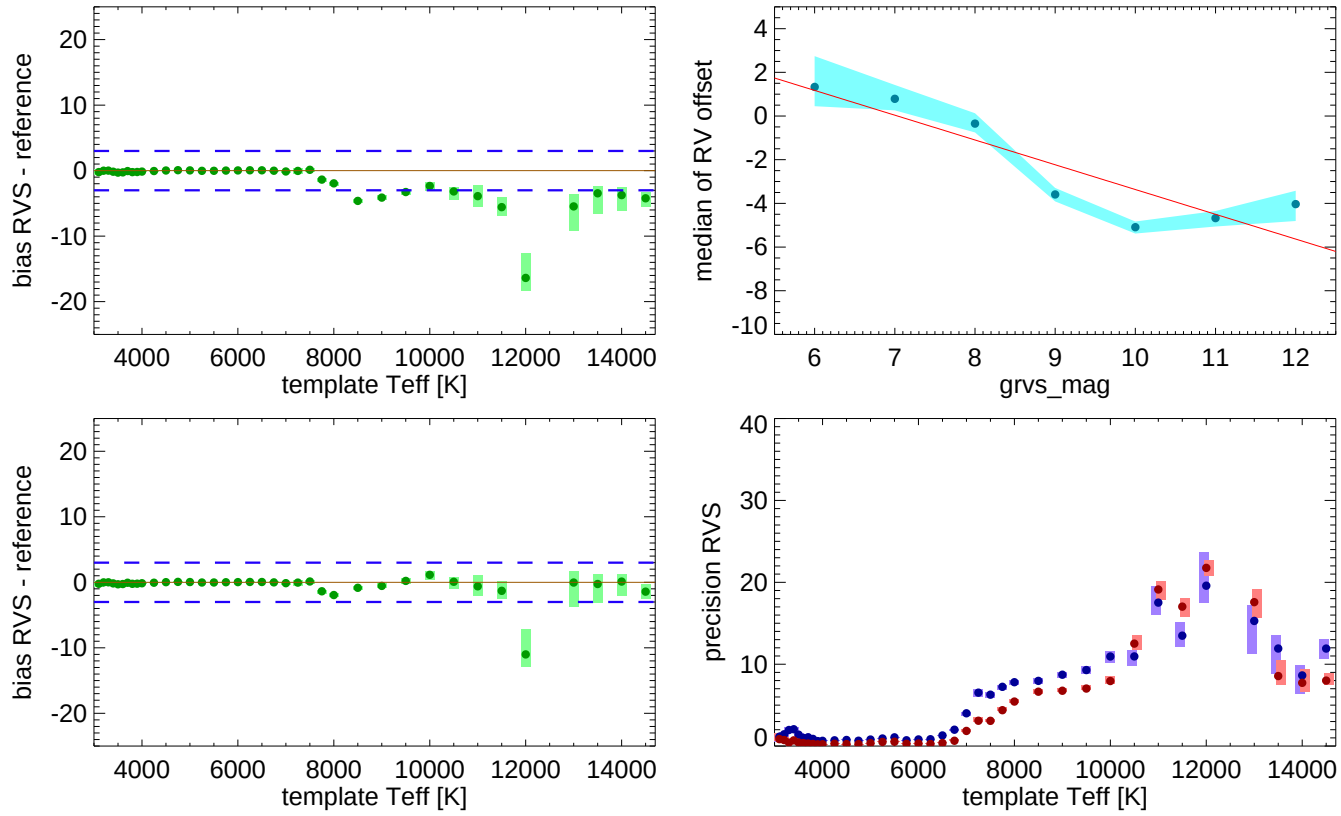

Fig. 6. Radial velocities compared to their reference values, where ReDetermineApHotStars has been applied to the hotter stars. The *top left panel* shows the bias of the radial velocity of the stars (RVS value minus reference value). It should be compared to the equivalent plot in Fig. 4 to see the improvement due to ReDetermineApHotStars. The dashed blue lines indicate $\pm 3\,\mathrm{km\,s^{-1}}$. The *top right panel* plots the median of the radial velocity bias of stars in the $T_{\mathrm{eff}} = 8500 - 14\,500$ K range, binned in one-magnitude-wide (`grvs_mag`) bins. The relation between the two is fitted linearly (red line). Applying the magnitude-related correction leads to an improved set of radial velocities, which are once again compared to their reference values (*bottom left panel*). The precision of these improved values is shown in the *bottom right panel*. Similarly to Fig. 4, the blue symbols give the external precision, and the red symbols give the internal precision. All plots include only stars with `grvs_mag` ≤ 12 mag.

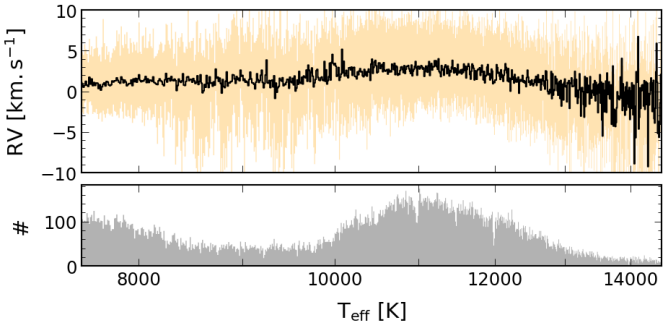

Fig. 7. Radial velocity shift that had to be applied by ESP-HS in CU8 to align the theoretical spectrum to the observed RVS spectrum as determined by MTA. It is plotted as a function of the T_{eff} determined by ESP-HS. The top panel shows the running median (computed over consecutive T_{eff} bins of 10 K) and the interquantile dispersion (15.85 % – 84.15 %) of this offset as a function of the effective temperature. The bottom panel shows how many stars went into each 10 K bin.

propriate mixture of Paschen and calcium lines, and therefore fits the observed spectrum much better. Using this template results in a more correct radial velocity. This radial velocity was used to place the DR3 archive spectrum (shown in Fig. 5) at its rest wavelength.

4. Results

4.1. Improved radial velocities

The top left panel of Fig. 6 shows the improvement in the bias of the radial velocities (RVS radial velocity minus the reference value). The offset of about $-20\,\mathrm{km\,s^{-1}}$ shown in Fig. 4 is reduced to about $-5\,\mathrm{km\,s^{-1}}$ for most of the effective temperature range.

The remaining $-5\,\mathrm{km\,s^{-1}}$ offset can be further reduced by considering the plot in the top right panel of Fig. 6. When we plot the bias of the radial velocities (for $T_{\mathrm{eff}} = 8500 - 14\,500$ K stars) as a function of magnitude (`grvs_mag`), a clear dependence on magnitude is seen. We approximate this dependence with a linear fit,

$$\mathrm{RV_{offset}} = 7.98 - 1.135 * \texttt{grvs\_mag}. \quad (1)$$

After we apply Eq. 1 to correct the radial velocities, we can again plot their bias (Fig. 6, bottom-left panel). Now, almost all points show a bias lower than $3\,\mathrm{km\,s^{-1}}$. The only exception is $T_{\mathrm{eff}} = 12\,000$ K; we were unable to determine why this temperature behaves somewhat differently. It is important to realise that the `radial_velocity` listed in the DR3 archive does not include this correction. It is up to the user of the DR3 hot-star radial velocities to decide whether they wish to apply this correction. As an example, we refer to Gaia Collaboration et al. (2022b), where this correction is applied.

The magnitude-dependent effect (Fig. 6, top right panel) is due to the difference in normalisation between the template and the observed spectrum. The normalisation consists of repeatedly fitting a second-degree polynomial to the fluxes and rejecting flux values that deviate too much from the polynomial. A stricter cutoff is used for fluxes below the polynomial than for those above it. Although the same technique is used for both the template and the observation, the presence of noise in the observation leads to a polynomial with a somewhat different slope than that of the noise-free template. With increasing effective temperature, the wider Paschen lines start to dominate, and radial velocity measurements become more sensitive to this slope mismatch, leading to a systematic offset. The effect becomes larger for the fainter stars because they have noisier observed spectra. For DR4 we are exploring a different normalisation technique where the normalised template is used as a reference for the normalisation of the observed spectrum. Preliminary indications are that this substantially reduces the magnitude-dependent effect described here.

The bottom right panel of Fig. 6 shows the two versions of the precision in the same way as for Fig. 4. With the improved method, both curves are now lower, indicating the improved precision. Furthermore, the internal precision (red curve) is now much closer to the external one. As for Fig. 4, we examined the influence of the uncertainty of the reference values on the external precision and found that it is negligible compared to the difference between external and internal precision. From the comparison of the two curves, we deduce that the `radial_velocity_error` is underestimated in the $T_{\rm eff}$ = 8000 − 10 000 K range by ∼30%. For higher temperatures ($T_{\rm eff}$ = 10 500 − 13 000 K), the `radial_velocity_error` is slightly overestimated (though the uncertainty regions of the two precisions partially overlap).

Figure 6 does not plot results for stars hotter than 14 500 K. These stars still present a considerable offset that could not be solved in DR3 and will be handled in DR4.

A further test of the hot-star radial velocities is provided by the CU8 processing to determine the astrophysical parameters from the spectra delivered by CU6. As part of the astrophysical parameter determination performed by the Extended Stellar Parameterizer - Hot Stars (ESP-HS; Creevey et al. 2022), the spectra are compared to synthetic spectra. When RVS data are available, the ESP-HS performs a first estimation of the astrophysical parameters of hot stars from the analysis of BP/RP data and then applies a cross-correlation technique in Fourier space to measure any remaining radial velocity offset of the RVS spectrum relative to the corresponding interpolated theoretical one. The RVS spectra used by CU8 were shifted to their rest wavelength by the CU6 processing (Sect. 2.1.3), therefore no offset should remain in principle. This CU6 shift is based on the combination of the transit radial velocities, however, while the ESP-HS test looks at the single combined spectrum for the source. This can result in a somewhat different radial velocity, and thus the ESP-HS test provides an independent way of validating the correctness of the CU6 radial velocity determination.

The ESP-HS module applies the radial velocity offset it measures to proceed further with the astrophysical parameter determination by fitting both BP/RP and RVS data. While the value of this CU8 offset shift is not published in DR3, it is kept for validation purposes and provides an a posteriori check on the CU6 results. An interesting point of this test is that it can be applied to a much larger number of stars, as we do not need a reference value for the radial velocity. Figure 7 shows the variation in required shift with the effective temperature measured by

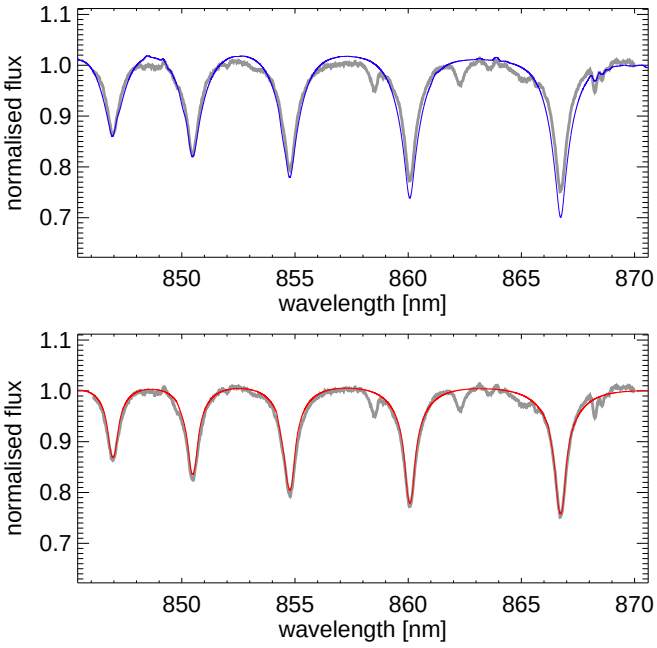

Fig. 8. Degeneracy between $T_{\rm eff}$ and metallicity for HDE 250290. The *top panel* shows a fit of the observed spectrum (grey) with a template (blue curve) corresponding closely to the parameters of Simón-Díaz et al. (2017, $T_{\rm eff}$ = 16 000 K, $\log g$ = 2.5 dex, [M/H] = 0.0 dex, and line-broadening velocity $v_{\rm broad}$ = 50 km s^{-1}). The *bottom panel* shows the fit with the template (red curve) as determined by ReDetermineApHotStars ($T_{\rm eff}$ = 6750 K, $\log g$ = 2.5 dex, [M/H] = −5.0 dex, and $v_{\rm broad}$ = 80 km s^{-1}).

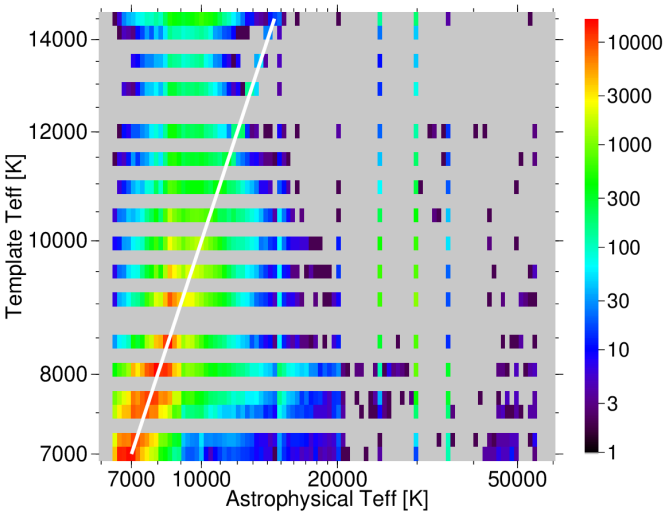

Fig. 9. Template $T_{\rm eff}$ as a function of the input astrophysical $T_{\rm eff}$. The colour scale gives the numbers of stars (on a logarithmic scale). The data are limited to those with `grvs_mag` ≤ 12 mag. The diagonal is indicated with a solid white line.

ESP-HS. Its median computed between 7500 K and 14 500 K is +1.7 km s^{-1}, with a half interquantile dispersion of 5.9 km s^{-1}. These values are low and are consistent with the results found from the comparison with the reference values (Fig. 6). The CU8 results thus confirm that the combined spectra are in the rest frame and that the CU6 determined radial velocities are accurate to within the claimed ±3 km s^{-1}. The median here has the opposite sign from that in Fig. 6 because this test measures the

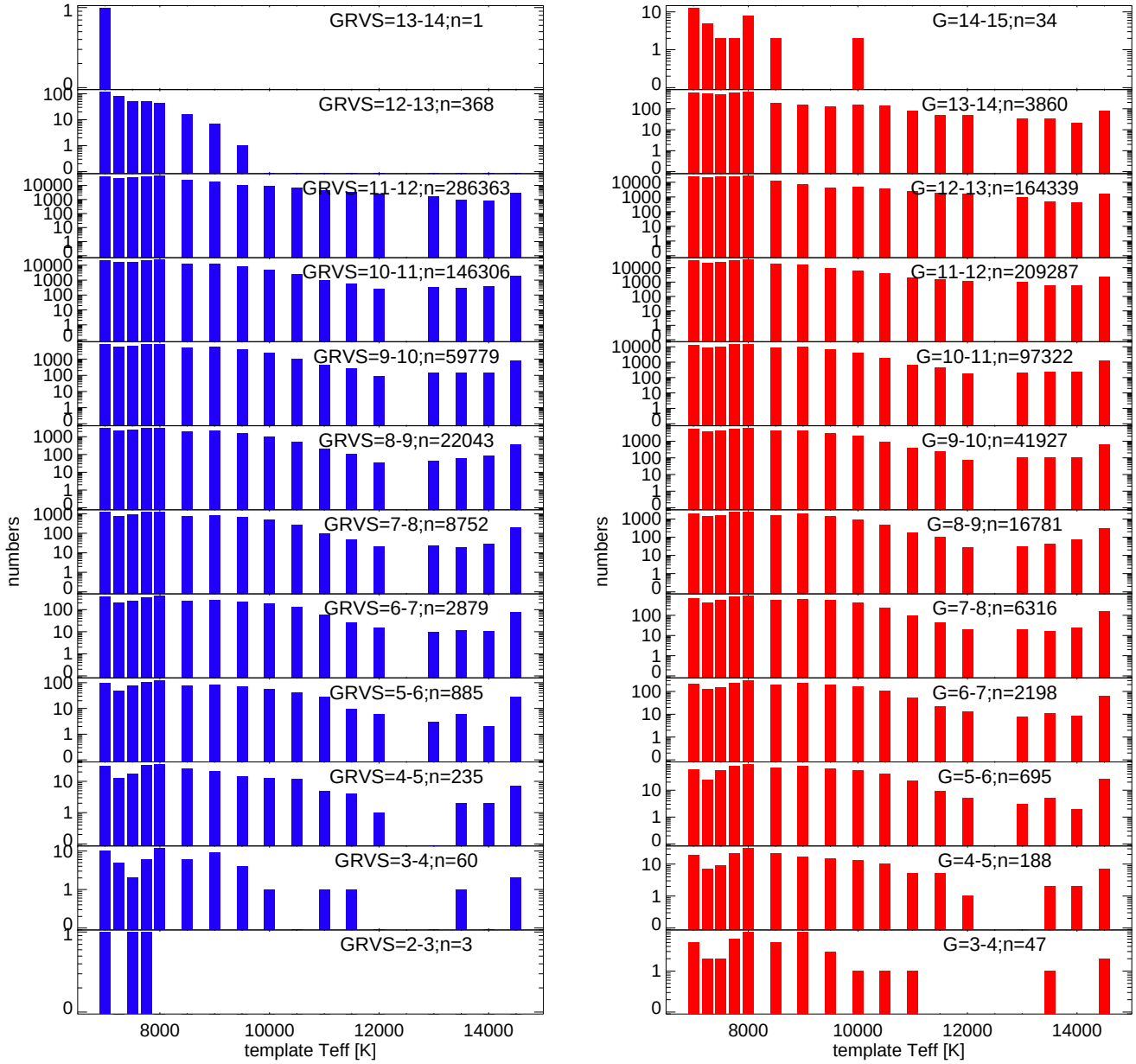

Fig. 10. Number of hot stars (log scale) with radial velocities in DR3, split up according to `rv_template_teff`, `grvs_mag` (left panel) and G magnitude (`phot_g_mean_mag`) (right panel). Each sub-panel lists the magnitude range and the number of stars within that range. While DR3 has a formal cutoff of magnitude 12, there are some stars fainter than this because of the difference between $G_{\rm RVS}$ and `grvs_mag` (see Sect. 3).

required shift of theoretical spectrum to align it to the observed spectrum.

4.2. Astrophysical versus template parameters

The improved selection of the best template does not necessarily mean that the DR3 template parameters (`rv_template_teff`, `rv_template_logg`, and `rv_template_fe_h` in the archive) describe the spectral type well. One effect that is responsible for this is the degeneracy between $T_{\rm eff}$ and metallicity in the very short wavelength range covered by RVS.

As an example of this degeneracy, Fig. 8 shows the RVS archive spectrum of the B3 Ib star Gaia DR3 3424656293035086208 = HDE 250290. The top panel fits the observation with a template that is as close as possible to the parameters listed by Simón-Díaz et al. (2017). The bottom plot uses the template from ReDetermineApHotStars. The Simón-Díaz et al. (2017) values are $T_{\rm eff}$ = 16 000 K, and we assume they used [M/H] = 0.0, as is appropriate for this hot Galactic star. The ReDetermineApHotStars result has a much lower $T_{\rm eff}$ (6750 K) and an extremely low metallicity ([M/H] = −5.0). Based on the RVS data alone, as shown in Fig. 8, the cooler template with the very low metallicity fits better. Only by using non-RVS data (as done by Simón-Díaz et al. (2017)) does it become clear that the [M/H] = −5.0 metallicity does not describe the atmospheric parameters of this star correctly.

A further illustration of the difference between the template parameters as used in the radial velocity determination and the astrophysical parameters is shown in Fig. 9. The astrophysical parameters used for this figure are the input parameters discussed in Sect. 2.1.1. The colour scale shows the number of stars having a specific combination of astrophysical and template $T_{\rm eff}$. Many

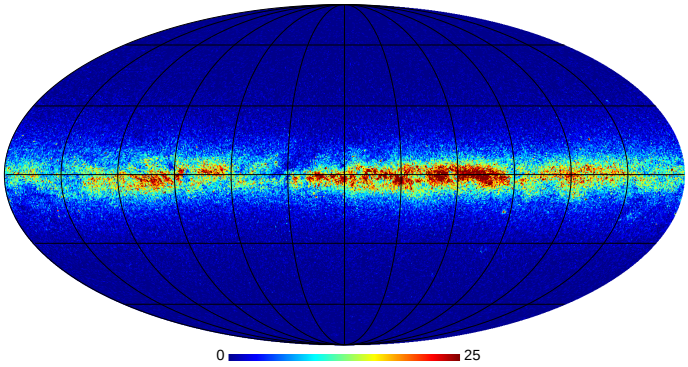

Fig. 11. Distribution on the sky (in Galactic coordinates) of the approximately half a million hot stars with DR3 radial velocities. The colour scale gives the number of stars per HEALpix of level 7.

stars lie close to the diagonal, and the two temperatures agree well. Some stars have a high astrophysical $T_{\rm eff}$, however, where ReDetermineApHotStars has assigned a low template $T_{\rm eff}$. Conversely, for stars with an astrophysical $T_{\rm eff} \approx 10\,000$ K, ReDetermineApHotStars sometimes finds a higher $T_{\rm eff}$. We stress again that the sole purpose of the template $T_{\rm eff}$ is to obtain the best possible radial velocity; it does not necessarily describe the astrophysical properties of the star well.

4.3. Hot stars with cool templates

As mentioned in Sect. 2.1.1, we were only able to use a preliminary version of the CU8 astrophysical parameters as input data. However, towards the end of the validation phase of the CU6 results, the CU8 results were available to us. These include the astrophysical parameters determined by the ESP-HS (Creevey et al. 2022). In these data, we found a number of stars for which we used a cool-star template for a star that is now classified by CU8 as a hot star.

This can again lead to a systematic offset because the calcium lines in the cool-star template try to fit the Paschen lines in the hot-star observed spectrum. We therefore carefully examined these cases again to determine which provided incorrect radial velocities. On the basis of this, the radial velocities of 20 470 hot stars (i.e. 3.8 % of all hot stars) with cool templates were removed from the DR3 archive.

4.4. Number of hot stars

The important difference between DR2 and DR3 discussed in this paper is the extension to 14 500 K of the effective temperature range for which radial velocities are determined. Of the total number of 33 812 183 of stars with radial velocities in DR3, 543 017 lie in the range `rv_template_teff` = 7000 – 14 500 K. The distribution of these hot stars with `rv_template_teff`, `grvs_mag` and G magnitude (`phot_g_mean_mag`) is shown in Fig. 10.

As expected, most of these stars are in the cooler, fainter part of the diagram. We introduced a formal cutoff in magnitude of `grvs_mag` = 12 mag, so that the S/N of the spectra is high enough for ReDetermineApHotStars to give good results. Some stars that are fainter than this cutoff are shown: this is due to the (sometimes) different value that was used by STA or MTA (see Sect. 3). Figure 10 has no stars with a template of 12 500 K because our list does not contain a synthetic spectrum with this $T_{\rm eff}$.

Figure 11 shows the distribution on the sky of the hot stars whose radial velocity is listed in DR3. As expected, the approximately half a million stars are concentrated in the disk of our Galaxy.

5. Conclusions

The third *Gaia* data release (*Gaia* DR3) is the first data release to contain radial velocities of stars with a template $T_{\rm eff}$ (`rv_template_teff`) between 7000 and 14 500 K. The archive contains 543 017 stars in this range.

A preliminary run of the pipeline deriving these hot-star radial velocities from the spectra of the Radial Velocity Spectrometer gave unsatisfactory results. The problem is due to the proximity to and systematic blueward offset of the calcium infrared triplet lines to the Paschen hydrogen lines. This leads to a systematic offset in radial velocity if the template does not describe the observed spectrum correctly. For this reason, a specific module was developed that improves the choice of the template. Using this module leads to a much better agreement between the *Gaia* radial velocities and the reference data. As a sufficiently high S/N is required for the module to be applied, the DR3 archive mostly contains only hot stars with `grvs_mag` $\leq$ 12 mag.

The user of the *Gaia* DR3 hot-star radial velocities should be aware of the following caveats. The template parameters $T_{\rm eff}$, $\log g$, and [M/H] used by CU6 (`rv_template_teff`, `rv_template_logg`, and `rv_template_fe_h` in the archive) are not necessarily a good description of the spectral type of the star. A magnitude-dependent effect is still present in the hot-star radial velocities of the *Gaia* DR3 archive. For stars with 8500 $\leq$ `rv_template_teff` $\leq$ 14 500 K and 6 $\leq$ `grvs_mag` $\leq$ 12 mag, this effect can be corrected for as follows:

$$\mathrm{RV}_{\rm corrected} = \texttt{radial\_velocity} - 7.98 + 1.135 * \texttt{grvs\_mag},$$

where `rv_template_teff`, `grvs_mag`, and `radial_velocity` are the quantities listed in the DR3 archive. This correction has been derived based on the median offsets of the DR3 radial velocities and the reference data. Individual stars can behave quite differently.

Acknowledgements

This work presents results from the European Space Agency (ESA) space mission Gaia. Gaia data are being processed by the Gaia Data Processing and Analysis Consortium (DPAC). Funding for the DPAC is provided by national institutions, in particular the institutions participating in the Gaia MultiLateral Agreement (MLA). The Gaia mission website is `https://www.cosmos.esa.int/gaia`. The Gaia archive website is `https://archives.esac.esa.int/gaia`. Acknowledgements are given in Appendix A. We thank Rosanna Sordo for comments on a preliminary version of this paper. This work has used the following software products: IDL (`https://www.l3harrisgeospatial.com/Software-Technology/IDL`), HEALPix (`https://healpix.sourceforge.io/`), Matplotlib (Hunter 2007, `https://matplotlib.org`), SciPy (Virtanen et al. 2020, `https://www.scipy.org`), and NumPy (Harris et al. 2020, `https://numpy.org`). This research has made use of the SIMBAD database, operated at CDS, Strasbourg, France.

References

Andrae, R., Fouesneau, M., Sordo, R., et al. 2022, A&A, submitted

Blomme, R., Edvardsson, B., Eriksson, K., et al. 2017, Gaia Data Processing and Analysis Consortium (DPAC) technical note GAIA-C6-TN-ROB-RHB-005, https://www.cosmos.esa.int/web/gaia/public-dpac-documents

Creevey, O., Sordo, R., Pailler, F., et al. 2022, A&A, submitted

Cropper, M., Katz, D., Sartoretti, P., et al. 2018, A&A, 616, A5

Damerdji, Y., Gosset, E., Morel, T., & et al. 2022, A&A, in prep.

David, M., Blomme, R., Frémat, Y., et al. 2014, A&A, 562, A97

De Angeli, F., Weiler, M., Montegriffo, P., et al. 2022, A&A, submitted

Eyer, L., Audard, M., Holl, B., & et al. 2022, A&A, in prep.

Frémat, Y., Royer, F., Marchal, O., et al. 2022, A&A, submitted

Gaia Collaboration, Brown, A. G. A., & Vallenari, A. 2022a, A&A

Gaia Collaboration, Brown, A. G. A., Vallenari, A., et al. 2018, A&A, 616, A1

Gaia Collaboration, Brown, A. G. A., Vallenari, A., et al. 2021, A&A, 649, A1

Gaia Collaboration, Brown, A. G. A., Vallenari, A., et al. 2016a, A&A, 595, A2

Gaia Collaboration, Drimmel, R., Romero-Gómez, M., et al. 2022b, A&A, submitted

Gaia Collaboration, Prusti, T., de Bruijne, J. H. J., et al. 2016b, A&A, 595, A1

Gosset, E., Damerdji, Y., Morel, T., & et al. 2022, A&A, in prep.

Gray, D. F. 2005, The Observation and Analysis of Stellar Photospheres (Cambridge University Press)

Harris, C. R., Millman, K. J., van der Walt, S. J., et al. 2020, Nature, 585, 357

Hunter, J. D. 2007, Computing in Science & Engineering, 9, 90

Katz, D., Sartoretti, P., Cropper, M., et al. 2019, A&A, 622, A205

Katz, D., Sartoretti, P., Guerrier, A., et al. 2022, A&A, in prep.

Recio-Blanco, A., de Laverny, P., Palicio, P., et al. 2022, A&A, submitted

Sartoretti, P., Blomme, R., David, M., & Seabroke, G. 2022a, Gaia DR3 documentation Chapter 6: Spectroscopy (https://gea.esac.esa.int/archive/documentation/GDR3/Data_processing/chap_cu6spe/)

Sartoretti, P., Katz, D., Cropper, M., et al. 2018, A&A, 616, A6

Sartoretti, P., Marchal, O., Babusiaux, C., et al. 2022b, A&A, submitted

Seabroke, G., Sartoretti, P., & et al. 2022, A&A, in prep.

Simón-Díaz, S., Godart, M., Castro, N., et al. 2017, A&A, 597, A22

Soubiran, C., Cantat-Gaudin, T., Romero-Gómez, M., et al. 2018, A&A, 619, A155

Virtanen, P., Gommers, R., Oliphant, T. E., et al. 2020, Nature Methods, 17, 261

Zucker, S. 2003, MNRAS, 342, 1291

[1] Royal Observatory of Belgium, Ringlaan 3, B-1180 Brussel, Belgium
[2] GEPI, Observatoire de Paris, Université PSL, CNRS, 5 Place Jules Janssen, F-92190 Meudon, France
[3] CNES Centre Spatial de Toulouse, 18 avenue Edouard Belin, F-31401 Toulouse Cedex 9, France
[4] Mullard Space Science Laboratory, University College London, Holmbury St Mary, Dorking, Surrey, RH5 6NT, United Kingdom
[5] Université Côte d'Azur, Observatoire de la Côte d'Azur, CNRS, Laboratoire Lagrange, Boulevard de l'Observatoire, CS 34229, 06304 Nice, France
[6] CRAAG - Centre de Recherche en Astronomie, Astrophysique et Géophysique, Route de l'Observatoire, Bp 63 Bouzareah, DZ-16340, Alger, Algérie
[7] Institut d'Astrophysique et de Géophysique, Université de Liège, 19c, Allée du 6 Août, B-4000 Liège, Belgium
[8] Observatoire astronomique de Strasbourg, Université de Strasbourg, CNRS, 11 rue de l'Université, F-67000 Strasbourg, France
[9] Centro de Astronomía, Universidad de Antofagasta, Avda. U. de Antofagasta, 02800 Antofagasta, Chile
[10] Universiteit Antwerpen, Onderzoeksgroep Toegepaste Wiskunde, Middelheimlaan 1, B-2020 Antwerpen, Belgium
[11] F.R.S.-FNRS, Rue d'Egmont 5, B-1000 Brussels, Belgium
[12] Leibniz Institute for Astrophysics Potsdam (AIP), An der Sternwarte 16, D-14482 Potsdam, Germany
[13] Laboratoire Univers et Particules de Montpellier, Université Montpellier, CNRS, Place Eugène Bataillon, CC72, F-34095 Montpellier Cedex 05, France
[14] Charles University, Faculty of Mathematics and Physics, Astronomical Institute of Charles University, V Holešovičkách 2, 180 00 Prague, Czech Republic
[15] Laboratoire d'astrophysique de Bordeaux, Université de Bordeaux, CNRS, B18N, allée Geoffroy Saint-Hilaire, F-33615 Pessac, France
[16] Faculty of Mathematics and Physics, University of Ljubljana, Jadranska ulica 19, SLO-1000 Ljubljana, Slovenia
[17] ATOS for CNES Centre Spatial de Toulouse, 18 avenue Edouard Belin, 31401 Toulouse Cedex 9, France
[18] Department of Astronomy and Theoretical Physics, Lund Observatory, Box 43, SE–221 00, Lund, Sweden
[19] Sorbonne Université CNRS, UMR 7095, Institut d'Astrophysique de Paris, 75014 Paris, France

Appendix A:

This work presents results from the European Space Agency (ESA) space mission Gaia. Gaia data are being processed by the Gaia Data Processing and Analysis Consortium (DPAC). Funding for the DPAC is provided by national institutions, in particular the institutions participating in the Gaia MultiLateral Agreement (MLA). The Gaia mission website is `https://www.cosmos.esa.int/gaia`. The Gaia archive website is `https://archives.esac.esa.int/gaia`.

The Gaia mission and data processing have financially been supported by, in alphabetical order by country:

- the Algerian Centre de Recherche en Astronomie, Astrophysique et Géophysique of Bouzareah Observatory;
- the Austrian Fonds zur Förderung der wissenschaftlichen Forschung (FWF) Hertha Firnberg Programme through grants T359, P20046, and P23737;
- the BELgian federal Science Policy Office (BELSPO) through various PROgramme de Développement d'Expériences scientifiques (PRODEX) grants and the Polish Academy of Sciences - Fonds Wetenschappelijk Onderzoek through grant VS.091.16N, and the Fonds de la Recherche Scientifique (FNRS), and the Research Council of Katholieke Universiteit (KU) Leuven through grant C16/18/005 (Pushing AsteRoseismology to the next level with TESS, GaiA, and the Sloan DIgital Sky SurvEy – PARADISE);
- the Brazil-France exchange programmes Fundação de Amparo à Pesquisa do Estado de São Paulo (FAPESP) and Coordenação de Aperfeicoamento de Pessoal de Nível Superior (CAPES) - Comité Français d'Evaluation de la Coopération Universitaire et Scientifique avec le Brésil (COFECUB);
- the Chilean Agencia Nacional de Investigación y Desarrollo (ANID) through Fondo Nacional de Desarrollo Científico y Tecnológico (FONDECYT) Regular Project 1210992 (L. Chemin);
- the National Natural Science Foundation of China (NSFC) through grants 11573054, 11703065, and 12173069, the China Scholarship Council through grant 201806040200, and the Natural Science Foundation of Shanghai through grant 21ZR1474100;
- the Tenure Track Pilot Programme of the Croatian Science Foundation and the École Polytechnique Fédérale de Lausanne and the project TTP-2018-07-1171 'Mining the Variable Sky', with the funds of the Croatian-Swiss Research Programme;
- the Czech-Republic Ministry of Education, Youth, and Sports through grant LG 15010 and INTER-EXCELLENCE grant LTAUSA18093, and the Czech Space Office through ESA PECS contract 98058;
- the Danish Ministry of Science;
- the Estonian Ministry of Education and Research through grant IUT40-1;
- the European Commission's Sixth Framework Programme through the European Leadership in Space Astrometry (ELSA) Marie Curie Research Training Network (MRTN-CT-2006-033481), through Marie Curie project PIOF-GA-2009-255267 (Space AsteroSeismology & RR Lyrae stars, SAS-RRL), and through a Marie Curie Transfer-of-Knowledge (ToK) fellowship (MTKD-CT-2004-014188); the European Commission's Seventh Framework Programme through grant FP7-606740 (FP7-SPACE-2013-1) for the Gaia European Network for Improved data User Services (GENIUS) and through grant 264895 for the Gaia Research for European Astronomy Training (GREAT-ITN) network;
- the European Cooperation in Science and Technology (COST) through COST Action CA18104 'Revealing the Milky Way with Gaia (MW-Gaia)';
- the European Research Council (ERC) through grants 320360, 647208, and 834148 and through the European Union's Horizon 2020 research and innovation and excellent science programmes through Marie Skłodowska-Curie grant 745617 (Our Galaxy at full HD – Gal-HD) and 895174 (The build-up and fate of self-gravitating systems in the Universe) as well as grants 687378 (Small Bodies: Near and Far), 682115 (Using the Magellanic Clouds to Understand the Interaction of Galaxies), 695099 (A sub-percent distance scale from binaries and Cepheids – CepBin), 716155 (Structured ACCREtion Disks – SACCRED), 951549 (Sub-percent calibration of the extragalactic distance scale in the era of big surveys – UniverScale), and 101004214 (Innovative Scientific Data Exploration and Exploitation Applications for Space Sciences – EXPLORE);
- the European Science Foundation (ESF), in the framework of the Gaia Research for European Astronomy Training Research Network Programme (GREAT-ESF);
- the European Space Agency (ESA) in the framework of the Gaia project, through the Plan for European Cooperating States (PECS) programme through contracts C98090 and 4000106398/12/NL/KML for Hungary, through contract 4000115263/15/NL/IB for Germany, and through PROgramme de Développement d'Expériences scientifiques (PRODEX) grant 4000127986 for Slovenia;
- the Academy of Finland through grants 299543, 307157, 325805, 328654, 336546, and 345115 and the Magnus Ehrnrooth Foundation;
- the French Centre National d'Études Spatiales (CNES), the Agence Nationale de la Recherche (ANR) through grant ANR-10-IDEX-0001-02 for the 'Investissements d'avenir' programme, through grant ANR-15-CE31-0007 for project 'Modelling the Milky Way in the Gaia era' (MOD4Gaia), through grant ANR-14-CE33-0014-01 for project 'The Milky Way disc formation in the Gaia era' (ARCHEOGAL), through grant ANR-15-CE31-0012-01 for project 'Unlocking the potential of Cepheids as primary distance calibrators' (UnlockCepheids), through grant ANR-19-CE31-0017 for project 'Secular evolution of galxies' (SEGAL), and through grant ANR-18-CE31-0006 for project 'Galactic Dark Matter' (GaDaMa), the Centre National de la Recherche Scientifique (CNRS) and its SNO Gaia of the Institut des Sciences de l'Univers (INSU), its Programmes Nationaux: Cosmologie et Galaxies (PNCG), Gravitation Références Astronomie Métrologie (PNGRAM), Planétologie (PNP), Physique et Chimie du Milieu Interstellaire (PCMI), and Physique Stellaire (PNPS), the 'Action Fédératrice Gaia' of the Observatoire de Paris, the Région de Franche-Comté, the Institut National Polytechnique (INP) and the Institut National de Physique nucléaire et de Physique des Particules (IN2P3) co-funded by CNES;
- the German Aerospace Agency (Deutsches Zentrum für Luft- und Raumfahrt e.V., DLR) through grants 50QG0501, 50QG0601, 50QG0602, 50QG0701, 50QG0901, 50QG1001, 50QG1101, 50QG1401, 50QG1402, 50QG1403, 50QG1404, 50QG1904, 50QG2101, 50QG2102, and 50QG2202, and the Centre for Information Services and High Performance Computing (ZIH) at

the Technische Universität Dresden for generous allocations of computer time;
- the Hungarian Academy of Sciences through the Lendület Programme grants LP2014-17 and LP2018-7 and the Hungarian National Research, Development, and Innovation Office (NKFIH) through grant KKP-137523 ('SeismoLab');
- the Science Foundation Ireland (SFI) through a Royal Society - SFI University Research Fellowship (M. Fraser);
- the Israel Ministry of Science and Technology through grant 3-18143 and the Tel Aviv University Center for Artificial Intelligence and Data Science (TAD) through a grant;
- the Agenzia Spaziale Italiana (ASI) through contracts I/037/08/0, I/058/10/0, 2014-025-R.0, 2014-025-R.1.2015, and 2018-24-HH.0 to the Italian Istituto Nazionale di Astrofisica (INAF), contract 2014-049-R.0/1/2 to INAF for the Space Science Data Centre (SSDC, formerly known as the ASI Science Data Center, ASDC), contracts I/008/10/0, 2013/030/I.0, 2013-030-I.0.1-2015, and 2016-17-I.0 to the Aerospace Logistics Technology Engineering Company (ALTEC S.p.A.), INAF, and the Italian Ministry of Education, University, and Research (Ministero dell'Istruzione, dell'Università e della Ricerca) through the Premiale project 'MIning The Cosmos Big Data and Innovative Italian Technology for Frontier Astrophysics and Cosmology' (MITiC);
- the Netherlands Organisation for Scientific Research (NWO) through grant NWO-M-614.061.414, through a VICI grant (A. Helmi), and through a Spinoza prize (A. Helmi), and the Netherlands Research School for Astronomy (NOVA);
- the Polish National Science Centre through HARMONIA grant 2018/30/M/ST9/00311 and DAINA grant 2017/27/L/ST9/03221 and the Ministry of Science and Higher Education (MNiSW) through grant DIR/WK/2018/12;
- the Portuguese Fundação para a Ciência e a Tecnologia (FCT) through national funds, grants SFRH/BD/128840/2017 and PTDC/FIS-AST/30389/2017, and work contract DL 57/2016/CP1364/CT0006, the Fundo Europeu de Desenvolvimento Regional (FEDER) through grant POCI-01-0145-FEDER-030389 and its Programa Operacional Competitividade e Internacionalização (COMPETE2020) through grants UIDB/04434/2020 and UIDP/04434/2020, and the Strategic Programme UIDB/00099/2020 for the Centro de Astrofísica e Gravitação (CENTRA);
- the Slovenian Research Agency through grant P1-0188;
- the Spanish Ministry of Economy (MINECO/FEDER, UE), the Spanish Ministry of Science and Innovation (MICIN), the Spanish Ministry of Education, Culture, and Sports, and the Spanish Government through grants BES-2016-078499, BES-2017-083126, BES-C-2017-0085, ESP2016-80079-C2-1-R, ESP2016-80079-C2-2-R, FPU16/03827, PDC2021-121059-C22, RTI2018-095076-B-C22, and TIN2015-65316-P ('Computación de Altas Prestaciones VII'), the Juan de la Cierva Incorporación Programme (FJCI-2015-2671 and IJC2019-04862-I for F. Anders), the Severo Ochoa Centre of Excellence Programme (SEV2015-0493), and MICIN/AEI/10.13039/501100011033 (and the European Union through European Regional Development Fund 'A way of making Europe') through grant RTI2018-095076-B-C21, the Institute of Cosmos Sciences University of Barcelona (ICCUB, Unidad de Excelencia 'María de Maeztu') through grant CEX2019-000918-M, the University of Barcelona's official doctoral programme for the development of an R+D+i project through an Ajuts de Personal Investigador en Formació (APIF) grant, the Spanish Virtual Observatory through project AyA2017-84089, the Galician Regional Government, Xunta de Galicia, through grants ED431B-2021/36, ED481A-2019/155, and ED481A-2021/296, the Centro de Investigación en Tecnologías de la Información y las Comunicaciones (CITIC), funded by the Xunta de Galicia and the European Union (European Regional Development Fund – Galicia 2014-2020 Programme), through grant ED431G-2019/01, the Red Española de Supercomputación (RES) computer resources at MareNostrum, the Barcelona Supercomputing Centre - Centro Nacional de Supercomputación (BSC-CNS) through activities AECT-2017-2-0002, AECT-2017-3-0006, AECT-2018-1-0017, AECT-2018-2-0013, AECT-2018-3-0011, AECT-2019-1-0010, AECT-2019-2-0014, AECT-2019-3-0003, AECT-2020-1-0004, and DATA-2020-1-0010, the Departament d'Innovació, Universitats i Empresa de la Generalitat de Catalunya through grant 2014-SGR-1051 for project 'Models de Programació i Entorns d'Execució Parallels' (MPEXPAR), and Ramon y Cajal Fellowship RYC2018-025968-I funded by MICIN/AEI/10.13039/501100011033 and the European Science Foundation ('Investing in your future');
- the Swedish National Space Agency (SNSA/Rymdstyrelsen);
- the Swiss State Secretariat for Education, Research, and Innovation through the Swiss Activités Nationales Complémentaires and the Swiss National Science Foundation through an Eccellenza Professorial Fellowship (award PCEFP2_194638 for R. Anderson);
- the United Kingdom Particle Physics and Astronomy Research Council (PPARC), the United Kingdom Science and Technology Facilities Council (STFC), and the United Kingdom Space Agency (UKSA) through the following grants to the University of Bristol, the University of Cambridge, the University of Edinburgh, the University of Leicester, the Mullard Space Sciences Laboratory of University College London, and the United Kingdom Rutherford Appleton Laboratory (RAL): PP/D006511/1, PP/D006546/1, PP/D006570/1, ST/I000852/1, ST/J005045/1, ST/K00056X/1, ST/K000209/1, ST/K000756/1, ST/L006561/1, ST/N000595/1, ST/N000641/1, ST/N000978/1, ST/N001117/1, ST/S000089/1, ST/S000976/1, ST/S000984/1, ST/S001123/1, ST/S001948/1, ST/S001980/1, ST/S002103/1, ST/V000969/1, ST/W002469/1, ST/W002493/1, ST/W002671/1, ST/W002809/1, and EP/V520342/1.

The GBOT programme uses observations collected at (i) the European Organisation for Astronomical Research in the Southern Hemisphere (ESO) with the VLT Survey Telescope (VST), under ESO programmes 092.B-0165, 093.B-0236, 094.B-0181, 095.B-0046, 096.B-0162, 097.B-0304, 098.B-0030, 099.B-0034, 0100.B-0131, 0101.B-0156, 0102.B-0174, and 0103.B-0165; and (ii) the Liverpool Telescope, which is operated on the island of La Palma by Liverpool John Moores University in the Spanish Observatorio del Roque de los Muchachos of the Instituto de Astrofísica de Canarias with financial support from the United Kingdom Science and Technology Facilities Council, and (iii) telescopes of the Las Cumbres Observatory Global Telescope Network.